Rapid design and modelling of wideband sinuous antenna reflector feeds through blended rational interpolation

Received 15 December, 2017; | Revised <day> <Month>, <year>; | Accepted <day> <Month>, <year>

DOI: xxx/xxxx

RESEARCH ARTICLE

Rapid design and modelling of wideband sinuous antenna reflector feeds through blended rational interpolation.

Annie Cuyt[1] | Ridalise Louw[2] | Christophe Segers[1] | Dirk de Villiers*[2]

[1]Departement WIS-INF, Universiteit Antwerpen, Antwerp, Belgium
[2]Department of Electrical and Electronic Engineering, Stellenbosch University, Stellenbosch, South Africa

Correspondence
*Dirk de Villiers, Room E407, Department of E&E Engineering, Stellenbosch Univeristy, 7600. Email: ddv@sun.ac.za

Abstract

This paper describes the design of sinuous antenna reflector feeds using blended rational interpolation. The blended rational interpolation method is developed to interpolate a sparse set of high-fidelity (HF) data while following the trends of a denser set of low-fidelity (LF) data. The HF data are obtained by full-wave computational electromagnetics simulations of the input impedance of a pyramidal sinuous antenna above a ground plane, while the LF data are obtained, at a significantly reduced computational cost, through simulations of a truncated version of the same antenna. Comparisons with other interpolation schemes, both for HF as well as for multi-fidelity data sets, are presented. It is shown that the blended rational interpolation scheme presented herein yields improved accuracy in most cases. A design example is also presented where a global model of the maximum input reflection coefficient over frequency is built over the design space, and thus used to identify the region of acceptable performance. Comparisons with a validation set of HF data resulted in similar results, with the blended rational interpolation model requiring significantly shorter computer simulation time.

KEYWORDS:
sinuous antenna, broadband antenna, reflector feed, radio astronomy antennas, rational interpolation, multi-fidelity modelling

1 | INTRODUCTION

Very wide bandwidth and low loss feed antennas for reflector systems have recently found application in modern radio telescopes such as the Allen telescope array [1] and the Square Kilometre Array (SKA) [2]. A popular class of feed antennas for such systems employs log-periodic geometries to achieve (quasi) frequency independent performance, while using inclined metallic surfaces over ground planes [3,4] to provide a uni-directional beam with a stable phase center. These antennas relax the classical constraint of a self-complementary geometry — which is known to provide a near constant input impedance and bi-directional radiation pattern [5] — in order to achieve the uni-directional radiation characteristics without the use of absorbing cavities (which result in a 3 dB loss). Recently, a sinuous type antenna was demonstrated [6] to be a possible candidate as feed for the SKA reflector system [7]. However, due to the inherent wide bandwidth and multi-scale properties of these types of antennas, the simulation time with full-wave computational electromagnetic (CEM) tools is often prohibitively slow for design and analysis tasks requiring a large amount of evaluations of the structure for a variety of frequencies and geometric parameters. In order to formally optimise a design of such a structure, one requires a significantly faster model of the responses of interest than that provided by full-wave CEM simulations.

In this paper we present a modelling strategy tailored specifically to the design of non-self-complementary log-periodic antennas. The idea relies on the availability of a faster low-fidelity (LF) model of the actual high-fidelity (HF) simulation model. Given the log-periodic nature of the antenna geometry, it is expected that the performance will be relatively smooth in the centre of the band, while degradation of both the impedance as well as radiation pattern performance is expected near the band edges due to mainly the truncation of the periodic structure. An LF model can thus be constructed to mimic the performance of the actual HF model only near the band edges — the regions where performance degradation is expected. Practically, this means that instead of simulating the full bandwidth CEM model, a narrower bandwidth model

with the same geometric parameters, and truncated to have the same lower or upper operating frequency limit, can be simulated instead. It is expected that the performance around the band edges of the LF and HF models should be similar, and also exhibit similar variations due to geometric changes.

The LF models constructed in this manner will still require a significant time to simulate, and will exhibit some differences from the HF models. We therefore employ a new multi-fidelity rational interpolation scheme to be able to smoothly and accurately model the input impedance of the antenna on a parameter space of interest. The rational model is constructed such that it interpolates whatever HF data is available, while following the trends of the LF data which are, by construction, more finely sampled than the HF data. To this end we start with a classical barycentric rational function description, which allows for well-defined constraints on the weights to allow a pole-free interpolation function. This model is extended to approximate the LF data in a least squares sense, while still interpolating all the HF data. The simple Lagrange form of the rational function leads to weight constraints which, in many cases, are too restrictive to allow the interpolant to follow the LF trends between the interpolating HF data points. We therefore suggest here a new blended rational interpolation strategy, which employs Bernstein polynomials as local approximations of the LF data, in order to remove the responsibility of following the LF trend behaviour from the weights. Local models are blended together globally by B-spline functions, the supports of which are restricted to the region of the local models. In this way, we are able to define a barycentric rational interpolation function with only a positive value constraint on the weights to ensure pole-free behaviour. The basic idea was first described in a recent conference paper [8], where only one-dimensional real output data were considered. Here, we expand the model to handle complex output data as well as higher dimensional input spaces.

The paper is organised to first describe the antenna problem at hand in terms of the antenna geometry as well as the performance metrics of interest. Thereafter the new blended rational interpolation scheme is described and illustrated using an example sinuous antenna. Then, the accuracy of the interpolation model is tested for a wide variety of examples against a range of other HF and multi-fidelity modelling schemes, where it is found that the method suggested here provides the most accurate models in most cases. Finally a design example is presented to show the utility of the method for a practical antenna design problem.

2 | ANTENNA DESCRIPTION

The antenna problem of interest here involves a conductor backed pyramidal sinuous antenna used as a reflector antenna feed. Specific performance metrics of interest, as well as a geometrical description of the antenna system, is provided in this section. Furthermore, a discussion on the slow simulation time — and the subsequent difficulty in designing the antenna — is provided, along with a description and justification of a faster, but inevitably less accurate, LF antenna model. This model is then used in the rest of the paper to estimate the actual (or HF) reflection response of the antenna over wide frequency and geometrical parameter ranges.

2.1 | Performance metrics

The design application presented here is a feed antenna for the reflector system of the SKA radio telescope [7]. Design of reflector feed antennas typically involves finding an antenna geometry that results in a primary radiation pattern which illuminates the reflector so as to maximise the gain G of the system, while simultaneously controlling the energy spilling past the reflector system which results in radiometric noise entering the system and a subsequent increase in noise temperature T. In addition, the antenna impedance should be matched to the driving source or load. Designing an antenna to operate optimally over a wide frequency bandwidth thus requires a large number of goal function evaluations (CEM simulations) to adequately explore the frequency variations and design space. We therefore seek fast and accurate models of the design goals to make this problem tractable.

The radiation pattern response should maximise the so-called receiving sensitivity (proportional to G/T used in communication system antennas), which is the ratio of effective aperture area and the total system noise A_e/T_{sys}. The calculation of this performance metric has been discussed by many workers, where comprehensive treatments can be found in [9,10,11]. Some recent papers [12,13] present accelerated methods for the calculation of the system temperature, and the methods discussed therein will be used in this work for all the receiving sensitivity calculations.

At the same time, the reflection coefficient magnitude response should, as usual, be below some specified value. Rational function interpolation models of input impedance as a function of frequency are widely used because of their physical relevance to circuit models and electromagnetic wave phenomena [14]. By extension, rational functions may also be well suited to interpolate variations over geometrical parameters of antenna structures since, numerically, they can capture steep variations in the response, and physically, antenna geometry variations often relate to frequency variations through the electrical size variations of the structure (e.g. the length of a thin wire dipole).

2.2 | Antenna geometry

Fig. 1 shows the geometry of the specific sinuous antenna considered here, which was previously presented in [15,6,8], and repeated here for clarity. The geometry is parametrised with the angles θ, α, and δ, the growth rate $\tau = d_n/d_{n+1}$, as well as the height above the ground plane h. The operating bandwidth of the antenna is controlled by the truncations at $d_1 = \lambda_h/8(\delta+\alpha)$ and $d_N = 1.2\lambda_l/4(\delta+\alpha)$, where N is the total number of log-periodic cells, and λ_h and λ_l indicate the wavelength corresponding to the maximum and the minimum operating frequencies respectively. The ground plane size is selected equal to the maximum projected diameter of the antenna, and the dual polarisation

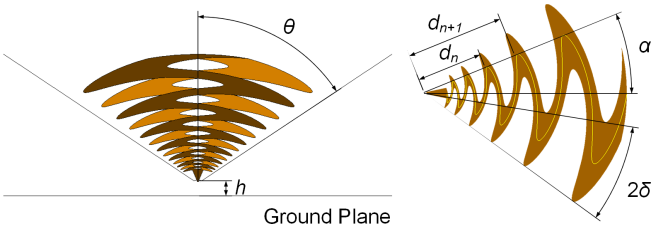

FIGURE 1 Geometry and design parameters of the sinuous antenna, showing a side projection in the left panel, and a top projection of one of the four petals in the right panel.

simulation edge port detail is shown in Fig. 2 . During the design phase a differential edge port is preferred for the simulations to simplify the geometry, and details on the design of a balanced wire feed can be found in [15], where comparisons between simulations and measurements are also provided.

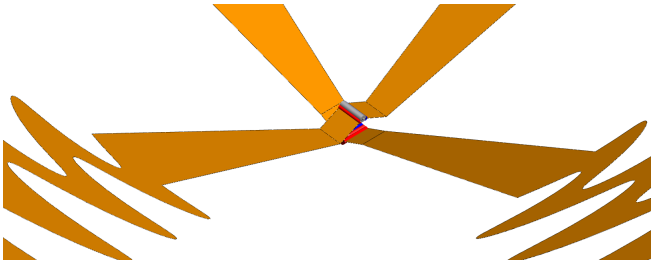

FIGURE 2 Dual polarisation differential simulation feed detail. Ground plane not shown for clarity.

In previous work [15,6], the antenna was designed by evaluating a relatively coarse grid of frequencies and design parameters, and simply selecting the best available version from this limited set. The reason is due to the prohibitively slow simulation times required for wide band versions of this antenna — in the order of several hours for $3:1$ bandwidth, and several days for $6:1$ bandwidth on a typical workstation. This is due to the inherent wideband and multi-scale nature of the structure, which requires a large number of discretisation unknowns in the simulation. To speed up the design process, a lower fidelity (coarse) model was suggested in [8], which is significantly faster to simulate, but still captures the important variations in the antenna performance — although at an inevitably reduced accuracy. The following section describes development of the LF model, and provides some information on simulation times and accuracy.

2.3 | Fast low-fidelity antenna model

Consider the sinuous antenna, designed to operate over the $[350, 1050]$ MHz bandwidth, with parameters $\tau = 0.7825$, $\alpha = 22.5°$, $\delta = 13.5°$, $\theta = 53°$ and $h = 5$ mm. Two LF models are also constructed with the same geometrical parameters, but with operating bandwidths of $2:1$ in $[350, 700]$ MHz and $[525, 1050]$ MHz, termed the low band and the high band models respectively. The input reflection coefficient responses of all three models are shown in Fig. 3 . As with all (quasi)

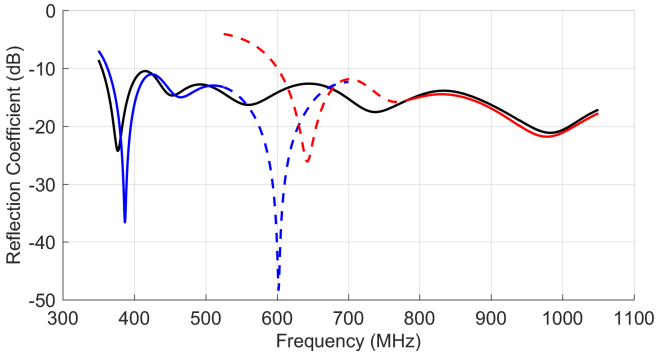

FIGURE 3 Comparison between the HF and LF model reflection coefficients. The blue line is the low band LF model, the red line the high band LF model, and the black line the HF model. Dashed lines indicate ignored edge effect regions in the coarse model frequency bands.

frequency independent antennas, the performance degrades near the band edges due to truncation effects, while in the middle of the operating band a logarithmic periodic response is observed. By simulating narrower bandwidth antennas as LF models, one can estimate the band edge performance of the actual HF antenna — which is exactly the region where the performance is degraded and therefore where the design goal is actually specified. Notice in Fig. 3 how the LF responses closely resemble the HF response in the region of their respective band edges, ie. the low frequencies for the low band LF model and the high frequencies for the high band model. The dashed lines indicate the edge effects of the LF models which are ignored, since they do not represent anything relating to the HF model. In all our LF models the antennas are *designed* to operate over a $2:1$ bandwidth (with the same design parameters as the HF model), but only simulated over the lower or upper half of the operating bandwidth for the low band and high band models respectively.

An illustration of the FEKO [16] simulation models is shown in Fig. 4 , where the typical mesh is overlayed onto the physical structure. For this

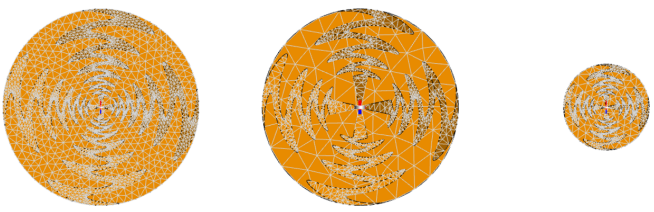

FIGURE 4 Comparison of the simulation meshes of the HF model (left), the low band LF model (centre) and the high band LF model (right).

example the mesh sizes and simulation times are reported in Table 1 , where a 5 times speedup is noticed for this modest bandwidth example.

TABLE 1 Comparison of HF and LF model simulation metrics.

	HF	LF low band	LF high band
Operating band (MHz)	$[350, 1050]$	$[350, 525]$	$[787.5, 1050]$
Mesh Cells	3746	2909	3544
Frequency samples	36	16	11
CPU time (hours)	3.12	0.345	0.376

In this case, the speedup is due mostly to the lower number of frequency samples required in the simulation, but, as the HF design bandwidth increases, this speedup factor increases exponentially since the LF models remains the same, while the number of mesh cells in the HF models scales as bandwidth squared.

Unfortunately, even though a significant speed up is observed for the LF models, the simulation times are still slow when a large number of designs must be investigated. Also, and more importantly, the responses of the LF and HF models are not identical, and may in fact show significant differences. A strategy is therefore sought to both correct and approximate the LF data, so that a fast and accurate model may be obtained for computationally expensive tasks such as design optimisation and sensitivity studies. The following section describes the required modelling strategy.

3 | RATIONAL INTERPOLATION SCHEME

The development presented here follows that presented in [8]. For clarity, and for the sake of notation, some of the basic concepts are repeated here. Emphasis is placed on the extensions to the previously presented method, namely interpolation of *complex* data over *multi-dimensional* parameter spaces. To facilitate the explanation of the mathematical development, an example data set is generated from a sinuous antenna, with parameters $\tau = 0.7825$, $\alpha = 22.5°$, $\delta = 13.5°$, $\theta = 53°$ and $h = 5$ mm. The low band LF model is used for this illustrative example which uses 5 HF interpolation data points, 36 LF data points, and 351 HF validation data points equally spaced in $[350, 525]$ MHz.

3.1 | Barycentric rational interpolation

Given complex data $f_i = f(x_i)$ at distinct real points $x_i \in [a, b], i = 0, \ldots, n$, a rational function $r_{n,w_0,\ldots,w_n}(x)$ interpolating $f(x)$ at the points x_i, may be constructed in the barycentric form

$$r_{n,w_0,\ldots,w_n}(x) = \frac{\sum_{i=0}^{n} w_i f_i \ell_i(x)}{\sum_{i=0}^{n} w_i \ell_i(x)} = \frac{\sum_{i=0}^{n} w_i f_i/(x - x_i)}{\sum_{i=0}^{n} w_i/(x - x_i)},$$

with $\ell_i(x) = \prod_{j=0, j\neq i}^{n}(x - x_j) = \ell(x)/(x - x_i)$ and $\ell(x) = \prod_{j=0}^{n}(x - x_j)$. The denominator is fixed by the location of the x_i and the numerator guarantees the interpolation property $r_{n,w_0,\ldots,w_n}(x_i) = f_i, i = 0, \ldots, n$, which holds for whatever w_i. The number of interpolation conditions is thus $n + 1$.

A necessary condition for $r_{n,w_0,\ldots,w_n}(x)$ to be polefree on the real axis, is $w_i w_{i+1} < 0$ [17]. For instance, it can be proven that the choice $w_i = (-1)^i$ guarantees a barycentric rational interpolant $r_{n,w_0,\ldots,w_n}(x)$ free of real poles. As a consequence no interpolation points can be unattainable [18], meaning that the model effectively interpolates every interpolation point.

A sufficient condition for weights $w_i = (-1)^i \omega_i$, with $\omega_i > 0$ and $a < x_0 < \ldots < x_n < b$, to guarantee a denominator free of poles on the real line [19], is given by

$$\begin{aligned} \frac{\omega_{j-1}}{b - x_{j-1}} &< \frac{\omega_j}{b - x_j}, \qquad j = 1, \ldots, n \\ \frac{\omega_j}{x_j - a} &> \frac{\omega_{j+1}}{x_{j+1} - a}, \qquad j = 0, \ldots, n-1. \end{aligned} \tag{1}$$

The interpolation model resulting from this strategy, where only the HF data are considered, is shown in Fig. 5 . It is clear that the interpolant does not follow the validation data very closely away from the sampled data.

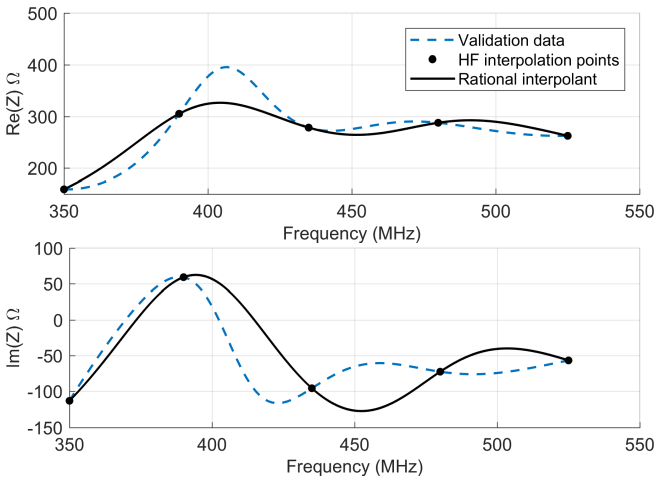

FIGURE 5 Barycentric rational interpolation of the input impedance as a function of frequency using only the HF data with $n + 1 = 5$.

Since we also have (more densely sampled and equidistant between consecutive HF points) data available from the LF model, we may use these to inform our selection of w_i such that the interpolant follows the *trend* of the LF data inbetween the (sparse) HF data points which are still interpolated. We denote the $m + 1$ LF data points by x_i^L and the $n +$

1 HF points by x_i^H. We also denote the values given at the points x_i^H by f_i^H and those given at x_i^L by f_i^L. Note that f_i^H at x_i^H can also be interpreted as a LF value at the same sample point. We incorporate the information provided by the LF data by solving a multi-fidelity form of the barycentric rational interpolation problem given by

$$r_{n,w_0,\ldots,w_n}(x) = \frac{\sum_{i=0}^n w_i f_i^H/(x-x_i^H)}{\sum_{i=0}^n w_i/(x-x_i^H)} \tag{2}$$

where the w_i satisfying (1) are given by

$$\arg\min_{w_0,\ldots,w_n} \sum_{j=0}^m \left| f_j^L - r_{n,w_0,\ldots,w_n}(x_j^L)\right|^2 \tag{3}$$

with $|\cdot|$ denoting the modulus of a complex value.

Condition (3) is a nonlinear optimisation problem, which can be linearised as

$$\arg\min_{w_0,\ldots,w_n} \sum_{j=0}^m \left| f_j^L \sum_{i=0}^n w_i/(x_j^L - x_i^H) - \sum_{i=0}^n w_i f_i^H/(x_j^L - x_i^H)\right|^2. \tag{4}$$

A similar approach, that however did not guarantee a polefree model, was presented in[20]. Although the formulas (2)-(3) or (2)-(4) express precisely what we expect from the computed rational model, the constraints (1) often restrict the search space for the least squares problems so much that the $w_0,\ldots,w_n$ resulting from the optimisation problem do not deliver a really good model. This is illustrated in Fig. 6 , where one can notice the interpolant failing to follow the LF data trends away from the HF interpolation points. So in practice, the method does not meet our expectations. This has encouraged us to look for an improvement.

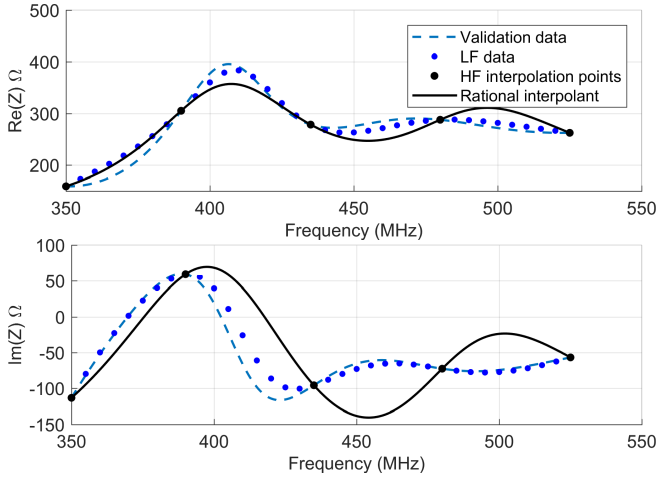

FIGURE 6 Barycentric rational interpolation of the input impedance as a function of frequency using the HF and LF data with $n+1=5$ and $m+1=36$.

3.2 | Blended rational interpolation of multi-fidelity data

We stick to the concept of the barycentric form which we want polefree, but preferably with a more relaxed condition than (1) on the weights in the expression. Therefore we turn our attention to blended models. Already the Lagrange form of a polynomial $p_n(x)$ of degree n, interpolating data f_i at points x_i for $i=0,\ldots,n$,

$$p_n(x) = \sum_{i=0}^n w_i f_i \ell_i(x), \quad w_i = 1/\prod_{j=0,j\neq i}^n (x_i - x_j),$$

can be considered as a simple blended model: the local interpolants f_i at x_i are blended together into a global interpolant by the blending functions $\ell_i(x)$ which by the choice of appropriate weights evaluate to 1 at the x_i. We explain how this idea can be applied to our problem statement.

Let the x_i^H be indexed such that $x_0^H < \ldots < x_n^H$ and let the x_i^L in the interval $[x_i^H, x_{i+1}^H]$ be denoted by $x_{i,0}^L < \ldots < x_{i,m_i}^L$ with $x_{i,0}^L = x_i^H, x_{i,m_i}^L = x_{i+1}^H$ and $\sum_{i=0}^{n-1}(m_i-1) = m+1$. Then we can first construct local models $p_i(x)$ exhibiting the trend indicated by the LF data in the interval $[x_i^H, x_{i+1}^H]$. By doing this we do not put the whole responsibility for the trend behaviour in the weights w_i. For the local models $p_i(x)$ we use a Bézier curve, as the LF data are collected at equidistant points in the interval $[x_i^H, x_{i+1}^H]$:

$$p_i(x) = \sum_{j=0}^{m_i} f_{ij}^L \beta_{ij}(z), \tag{5}$$
$$f_{ij}^L = f\left(x_{i,j}^L\right), \qquad z = \frac{x - x_i^H}{x_{i+1}^H - x_i^H},$$
$$\beta_{ij}(z) = \binom{m_i}{j} z^j (1-z)^{m_i - j}.$$

The local polynomial model $p_i(x)$ defined on the interval $[x_i^H, x_{i+1}^H]$, has the property that it interpolates in $x_{i,0}^L = x_i^H$ and $x_{i,m_i}^L = x_{i+1}^H$ and that it follows the trend given by the so-called control points $x_{i,1}^L < \ldots < x_{i,m_i-1}^L$ inbetween.

Afterwards these local models are then blended together by suitable blending functions, such as quadratic or cubic B-splines $B_{i,d}(x)$ where the degree $d = 2$ or 3. For $d=2$ it is defined by the knots $(x_{i-1,m_{i-1}-1}^L, x_i^H, x_{i+1}^H, x_{i+1,1}^L)$. Here $x_{i-1,m_{i-1}-1}^L$ and $x_{i+1,1}^L$ are respectively the LF points preceding x_i^H and following x_{i+1}^H. For $d=3$ we add the knot $(x_i^H + x_{i+1}^H)/2$ in the middle. To define the B-spline when $i=0$ or $i=n-1$, we add a virtual point outside the interval $[x_0^H, x_n^H]$ at approximately the same distance as the one between the LF points. With these knots, we know that $B_{i,d}(x)$ has support $[x_{i-1,m_{i-1}-1}^L, x_{i+1,1}^L]$. Fig. 7 illustrates the local models and blending functions, and how they relate to the LF and HF data.

This leads us to the rational expression, now having a piecewise polynomial numerator and denominator, of the form

$$R_{n,w_0,\ldots,w_{n-1}}(x) = \frac{\sum_{i=0}^{n-1} w_i p_i(x) B_{i,d}(x)}{\sum_{i=0}^{n-1} w_i B_{i,d}(x)}. \tag{6}$$

With $d=2$ the function $R_{n,w_0,\ldots,w_{n-1}}(x)$ is continuously differentiable. With $d=3$ it is twice continuously differentiable. Because $x_i^H - x_{i-1,m_{i-1}-1}^L < x_i^H - x_{i-1}^H$ and $x_{i+1,1}^L - x_{i+1}^H < x_{i+2}^H - x_{i+1}^H$, use

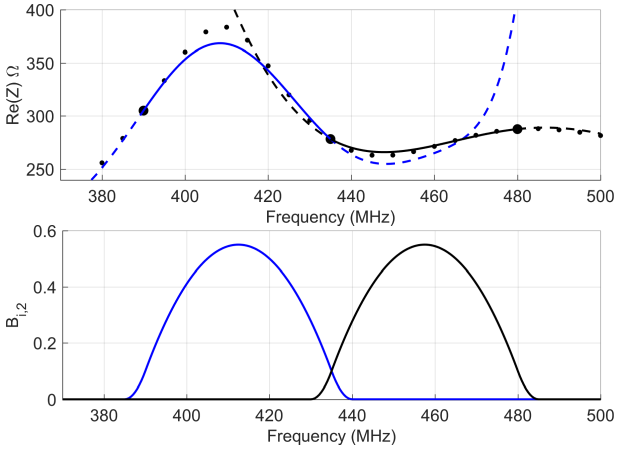

FIGURE 7 Local models p_i (top panel) and blending functions $B_{i,2}$ (bottom panel) used in the blended rational interpolation scheme. Small dots indicate the LF data and large dots the HF data — both sets taken from the middle two intervals of the top panel of Fig. 6 . The blue curves represent the functions relating to the interval between the first two HF data points, and black curves those relating to the interval between the last two HF data points. Solid lines indicate the local models on their relevant domains, while dashed lines indicate the extensions of the local models outside the relevant intervals.

of the LF points as knots restricts the influence of $p_i(x)$ almost solely to the interval $[x_i^H, x_{i+1}^H]$, as can be seen in Fig. 7 . The latter is important when HF points are spread far apart. Since the functions $B_{i,d}(x)$ are positive, it is sufficient to impose that

$$w_i > 0, \qquad i = 0, \ldots, n-1 \tag{7}$$

to make $R_{n,w_0,\ldots,w_{n-1}}(x)$ polefree on the real axis. Because $p_i(x_i^H) = f_i, p_i(x_{i+1}^H) = f_{i+1}, i = 0, \ldots, n-1$ we know that the model $R_{n,w_0,\ldots,w_{n-1}}(x)$ also interpolates in every HF point x_i^H:

$$R_{n,w_0,\ldots,w_{n-1}}(x_0^H) = \frac{w_0 p_0(x_0^H) B_{0,d}(x_0^H)}{w_0 B_{0,d}(x_0^H)} = f_0^H,$$

$$R_{n,w_0,\ldots,w_{n-1}}(x_i^H) = \frac{\sum_{k=i-1}^{i} w_k p_k(x_i^H) B_{k,d}(x_i^H)}{\sum_{k=i-1}^{i} w_k B_{k,d}(x_i^H)} = f_i^H, \quad 0 < i < n,$$

$$R_{n,w_0,\ldots,w_{n-1}}(x_n^H) = \frac{w_{n-1} p_{n-1}(x_n^H) B_{n-1,d}(x_n^H)}{w_{n-1} B_{n-1,d}(x_n^H)} = f_n^H.$$

The weights in (6), restricted to (7), are taken to be the solution of the least squares problem

$$\arg \min_{w_0,\ldots,w_{n-1}} \sum_{i=0}^{n-1} \sum_{j=0}^{m_i} \left| f_{i,j}^L - R_{n,w_0,\ldots,w_{n-1}}(x_{i,j}^L) \right|^2 \tag{8}$$

or

$$\arg \min_{w_0,\ldots,w_{n-1}} \sum_{i=0}^{n-1} \sum_{j=0}^{m_i} \left| f_{ij}^L \sum_{k=0}^{n-1} w_k B_{k,d}(x_{i,j}^L) - \sum_{k=0}^{n-1} w_k p_k(x_{i,j}^L) B_{k,d}(x_{i,j}^L) \right|^2. \tag{9}$$

The sums for j running from 0 to m_i are actually sums for j from 1 to $m_i - 1$ as in the endpoints of each interval the function interpolates.

The model (6) with (7)-(5) and (8) or (9) gives significantly improved results, as illustrated in Fig. 8 , where the interpolant more closely follows the LF data trends between the HF interpolation points.

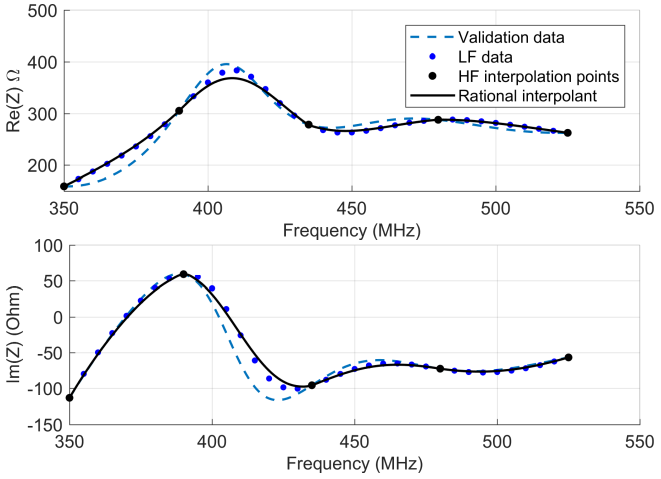

FIGURE 8 Blended rational interpolation of the input impedance as a function of frequency using the HF and LF data with $n + 1 = 5$ and $m + 1 = 36$.

3.3 | Extension to multi-dimensional parameter spaces

In this section we explain how to generalise our model to the case where the MF points are not real points anymore but real vectors in $\mathbb{R}^D$ ($D > 1$). For the sake of notation and without loss of generality, we restrict ourselves to $D = 2$ in the description.

Consider complex HF data f_{ij}^H at a grid of distinct real vectors

$$(x_i^H, y_j^H) \in [a_1, b_1] \times [a_2, b_2], \quad i = 0, \ldots, n_1, \quad j = 0, \ldots, n_2 \tag{10}$$

with $x_0^H < \ldots < x_{n_1}^H, y_0^H < \ldots < y_{n_2}^H$ and complex LF data $f_{(i,k_i),(j,l_j)}^L$ at a grid of distinct real vectors

$$(x_{i,k_i}^L, y_{j,l_j}^L) \in [a_1, b_1] \times [a_2, b_2], \quad i = 0, \ldots, n_1 - 1, \quad k_i = 0, \ldots, m_{i,1}, \quad j = 0, \ldots, n_2 - 1, \quad l_j = 0, \ldots, m_{j,2} \tag{11}$$

with $x_{i,0}^L < \ldots < x_{i,m_{i,1}}^L$ equidistant in $[x_{i,0}^L, x_{i,m_{i,1}}^L], x_{i,0}^L = x_i^H, x_{i,m_{i,1}}^L = x_{i+1}^H, i = 0, \ldots, n_1 - 1$ and similarly for the y-values. We want to find a model, similar to the one in the previous section, which interpolates the HF data and follows the trend of the LF data. To do this, we need to find multi-dimensional local models $p_{ij}(x)$ and multi-dimensional blending functions.

For the local models, we can use a multivariate form of the Bernstein polynomials [21]:

$$p_{ij}(x,y) = \sum_{k=0}^{m_{i,1}} \sum_{l=0}^{m_{j,2}} f^L_{(i,k),(j,l)} \beta_{(i,k),(j,l)}(u,v)$$
$$(u,v) = \left(\frac{x - x_i^H}{x_{i+1}^H - x_i^H}, \frac{y - y_j^H}{y_{j+1}^H - y_j^H} \right),$$
$$\beta_{(i,k),(j,l)}(u,v) = \beta_{ik}(u) \cdot \beta_{jl}(v).$$

The local model $p_{ij}(x,y)$ interpolates in the HF points from $\{x_i^H, x_{i+1}^H\} \times \{y_j^H, y_{j+1}^H\}$ and follows the trend given by the LF points in the rectangle with the HF points as corner points.

For the blending functions, we can simply use the tensor product of B-splines. Let for $d = 2$ or 3,

$$B_{i,j,d}(x,y) := B_{i,d}(x) \cdot B_{j,d}(y),$$

with support $[x^L_{i-1,m_{i-1,1}-1}, x^L_{i+1,1}] \times [y^L_{j-1,m_{j-1,2}-1}, y^L_{j+1,1}]$, where our notation is entirely analogous to the one introduced in the previous section.

Now we can easily write down the two-dimensional rational expression interpolating every HF data point:

$$R_{n,w}(x,y) = \frac{\sum_{i=0}^{n_1-1} \sum_{j=0}^{n_2-1} w_{ij} p_{ij}(x,y) B_{i,j,d}(x,y)}{\sum_{i=0}^{n_1-1} \sum_{j=0}^{n_2-1} w_{ij} B_{i,j,d}(x,y)}$$

with $w = (w_{ij})_{ij}, i = 0, \ldots, n_1 - 1, j = 0, \ldots, n_2 - 1$. It is again sufficient to impose

$$w_{ij} > 0, \quad i = 0, \ldots, n_1 - 1, \quad j = 0, \ldots, n_2 - 1 \tag{12}$$

to make $R_{n,w}(x,y)$ polefree in $\mathbb{R}^2$. The weights w_{ij}, restricted to (12), are given by

$$\arg\min_w \sum_{i=0}^{n_1-1} \sum_{j=0}^{n_2-1} \sum_{k=0}^{m_{i,1}} \sum_{l=0}^{m_{j,2}} \left| f^L_{(i,k),(j,l)} - R_{n,w}\left(x^L_{i,k}, y^L_{j,l}\right) \right|^2 \tag{13}$$

or the linearised

$$\arg\min_w \sum_{i=0}^{n_1-1} \sum_{i=0}^{n_2-1} \sum_{k=0}^{m_{i,1}} \sum_{l=0}^{m_{j,2}} \left| f^L_{(i,k),(j,l)} D_{n,w}\left(x^L_{i,k}, y^L_{j,l}\right) - N_{n,w}\left(x^L_{i,k}, y^L_{j,l}\right) \right|^2, \tag{14}$$

where we put

$$D_{n,w}(x,y) = \sum_{i=0}^{n_1-1} \sum_{j=0}^{n_2-1} w_{ij} B_{i,j,d}(x,y)$$

and

$$N_{n,w}(x,y) = \sum_{i=0}^{n_1-1} \sum_{j=0}^{n_2-1} w_{ij} p_{ij}(x,y) B_{i,j,d}(x,y).$$

An example of this blended multi-dimensional rational model is given in Fig. 9 . Here we use the same antenna as described previously for the frequency variations, but we also vary the geometric parameter $\theta \in [47°, 59°]$. In this case we select the HF and LF data on 5×3 and 36×13 grids respectively, while the HF validation data is calculated on a 3×2 grid in between the training samples. The interpolant closely follows the HF validation data. The accuracy of the blended rational model described here will be evaluated for a range of sinuous antenna examples in the following section.

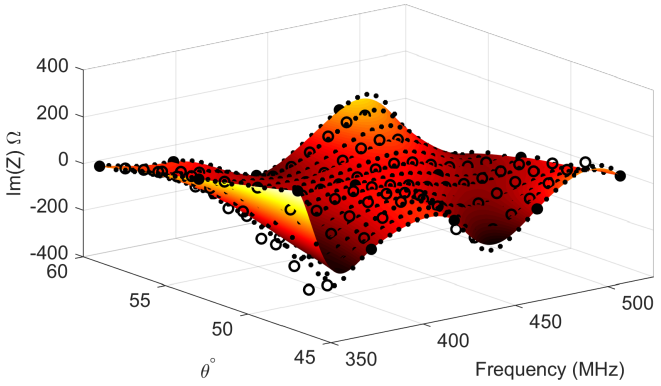

FIGURE 9 Blended rational interpolation of the imaginary part of the input impedance using the HF and LF 2-D data. HF data are indicated by large dots, LF data by small dots, validation data by open circles, and the resulting rational interpolant by the surface.

4 | APPLICATION EXAMPLES

This section evaluates the accuracy and demonstrates the utility of the suggested modelling scheme. First, a collection of the pyramidal sinuous antennas are simulated using various parameter ranges and sample densities, and the accuracy of the blended rational interpolation is compared to several other modelling schemes. Thereafter, a design example is presented to illustrate how the suggested method can be used to accelerate the design of an antenna in a realistic multi-objective design context.

4.1 | Modelling accuracy

To quantify the accuracy of the blended rational interpolation scheme presented here, we consider a range of 2-D sinuous antenna examples with bandwidths and simulation models as in Table 1 . Along with frequency, the geometric parameters are varied along four one-dimensional slices through the centre of the hypercube defined by $\tau \in [0.75, 0.9]$, $\delta/\alpha \in [0.4, 0.8]$, $\delta + \alpha \in [28°, 44°]$, and $\theta \in [47°, 59°]$. The number of LF data points along each dimension is fixed at $31, 41, 17, 13$, and 89 along frequency, τ, δ/α, $\delta + \alpha$, and θ, respectively. The number of HF data is varied on the LF grid to illustrate the effects of using coarser grids of HF data. In order to quantify the modelling errors, a validation set (full HF antenna simulation) is calculated everywhere on the LF data points, and only points not included in the HF data set are retained for error calculations.

As comparison, estimation of the input impedance is also performed using a variety of other interpolation methods. These include three methods operating only on the available HF data, namely spline, Kriging, and barycentric rational interpolation (see Sec. 3.1). In addition, co-Kriging was evaluated as a multi-fidelity interpolation method. For the Kriging and co-Kriging, the implementation in the ooDACE toolbox was used with default settings [22].

For all the examples the error metrics are the Average Euclidean Error (AEE), [23]

$$\mathrm{AEE}(y,\tilde{y}) = \frac{1}{M}\sum_{i=1}^{M} |y_i - \tilde{y}_i|\,, \tag{15}$$

and the maximum errors (MAX),

$$\mathrm{MAX}(y,\tilde{y}) = \max |y_i - \tilde{y}_i| \qquad i = 1,\ldots,M, \tag{16}$$

with y_i the verification and $\tilde{y}_i$ the predicted response values.

The resulting error plots are shown in Fig. 10 . In general it can be seen that the blended rational interpolation scheme suggested here performs better than the other modelling schemes — especially when the number of HF data is reduced. The mean values of the errors in Fig. 10 are summarised in Table 2 .

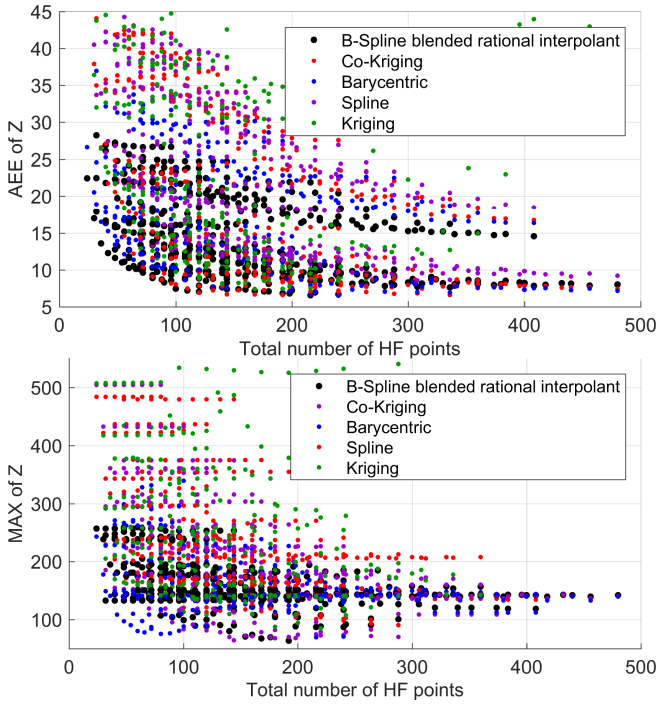

FIGURE 10 Comparisons of the modelling errors for a variety of modelling schemes and geometries as a function of the total number of HF data points. The average error is shown in the top panel and the maximum error in the bottom panel. Different modelling schemes are indicated by different colours.

TABLE 2 Mean values of all the errors in Fig. 10 .

	Data	AEE	MAX
Blended Rational Interpolant	HF/LF	14.2	157
co-Kriging	HF/LF	17.8	164
Kriging	HF	26.3	241
Barycentric Rational Interpolant	HF	22.7	199
Spline	HF	20.8	216

4.2 | Design example

As a design example, a pyramidal sinuous antenna geometry is sought which operates over the $[350, 1050]$ MHz bandwidth, with an input reflection coefficient smaller than -10 dB, and maximum receiving sensitivity when feeding the offset Gregorian reflector system used by the SKA [7]. Design parameters are limited to $\mathbf{x} = [\tau, \delta/\alpha]$, with $\delta + \alpha = 36°$ and $\theta = 53°$.

A blended rational interpolation model of the input impedance is built over the full 3-D design space (including frequency) using a $[22 \times 22 \times 5]$ grid of HF data points, and grids of $[41 \times 41 \times 36]$ and $[41 \times 41 \times 53]$ points for the low band and high band LF models respectively (grids ordered as $[\tau, \delta/\alpha, \text{frequency}]$). As previously, the low band and high band frequency ranges are $[350, 525]$ MHz and $[787.5, 1050]$ MHz respectively. Using this model, the worst case (maximum) absolute value of the input reflection coefficient is calculated across the geometric input space and plotted in Fig. 11 . To test the result, a verification set was calculated using a grid of $[41 \times 41 \times 176]$ HF models. The interpolant is seen to follow the verification data relatively well. The region where the reflection coefficient specification (< -10 dB) is met is plotted in Fig. 12 , where a good agreement between the rational interpolation model and the verification data is observed.

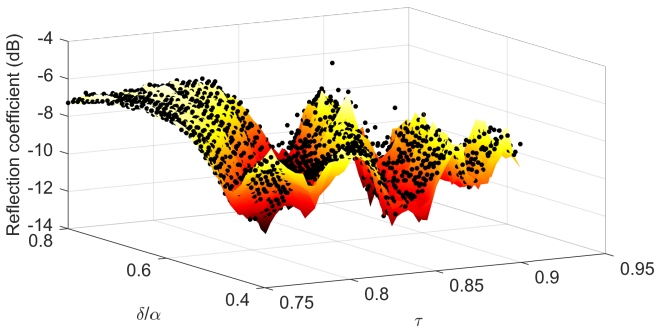

FIGURE 11 Worst case reflection coefficient over the geometrical design space. The surface shows the rational interpolant and the dots indicate a verification set.

The receiving sensitivity is modelled as described in [13], and an objective function is defined which returns the average receiving sensitivity in the band $[650, 1050]$ MHz (in order to reduce the influence of the high galactic noise in the lower end of the band [7] — see Fig. 14). A simple grid search is used to maximise the objective function over the region constrained by the acceptable reflection coefficient performance, and the optimal geometry is found to be $\tau = 0.874$ and $\delta/\alpha = 0.63$. This antenna was simulated and the results are shown in Figs. 13 and 14 .

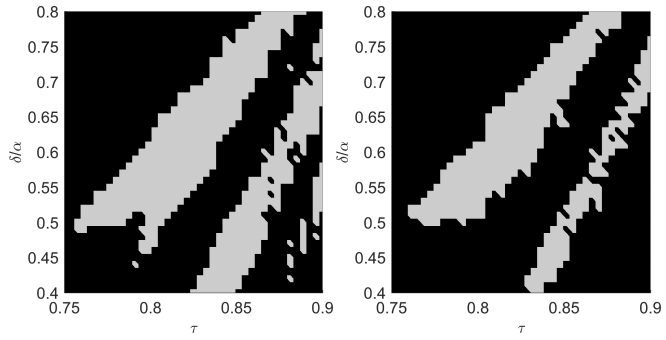

FIGURE 12 Regions where the worst case reflection coefficient is within the specification (< -10 dB) shown in light grey, with the rational interpolation model in the left panel and the verification set in the right panel.

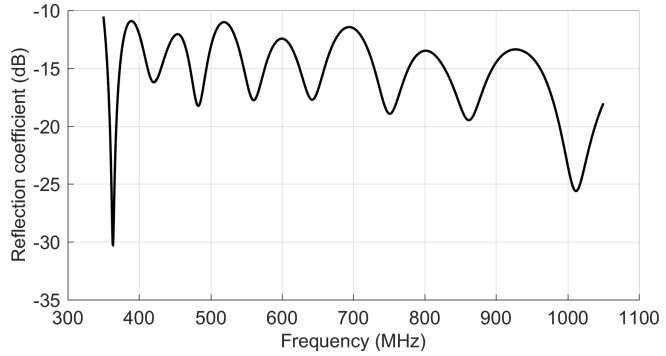

FIGURE 13 Reflection coefficient of the optimal design into a $237\ \Omega$ reference impedance.

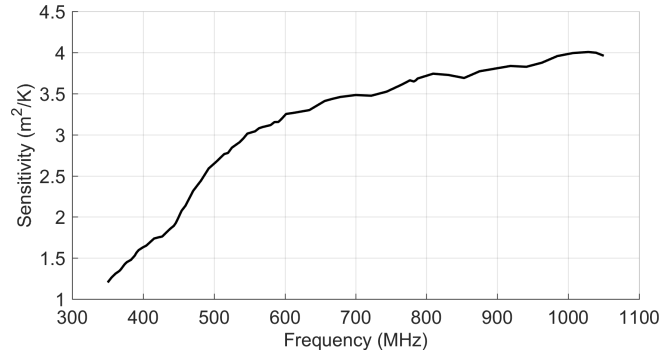

FIGURE 14 Receiving sensitivity of the optimal design.

The final reflection coefficient is well below the -10 dB level across the band, while the average receiving sensitivity in the band above 650 MHz is 3.71 m^2/K. Note how the sensitivity drops off steeply below 650 MHz due to the increasing sky temperature caused by galactic radiation.

5 | CONCLUSION

This paper presents a strategy to efficiently model the input impedance of a sinuous antenna for use as a reflector antenna feed. The method relies on the availability of both HF and LF data describing the input impedance of the antenna. LF data is obtained at a significantly reduced computational cost, when compared to the HF data, by CEM simulations of truncated versions of the antenna. Since the antenna is geometrically approximately log-periodic in nature, the truncated versions provide a good estimate of the performance at the operating frequency band edges, but are much faster to simulate due to the narrower frequency bandwidth, as well as reduced electrical size. In order to improve the accuracy of the LF data described above, a rational interpolation scheme is presented which interpolates a sparse set of HF data (the full antenna simulations), while following the trends of a denser set of LF data (the truncated antenna simulations). Several shortcomings of traditional barycentric rational interpolation formulations, including multi-fidelity ones, are addressed herein. These mainly relate to relaxing constraints on the interpolation weights to allow pole-free interpolants which still have the flexibility to follow the LF trends while interpolating the HF data with no unattainable points.

The method was applied on a variety of sinuous antennas to evaluate and compare the accuracy with a range of other interpolation methods, with results showing improved accuracy in most of the examples considered. A design example was also demonstrated, where an optimal design in terms of receiving sensitivity for a given reflection coefficient constraint was delivered using a significantly reduced set of HF models when compared to direct methods.

Future work on the rational interpolation method may include reformulating it to allow for scattered data sets, since the current formulation relies on regular grids of data which suffer from the curse of dimensionality for high dimensional models. Using scattered data sets also allows for sequential and adaptive sampling, which in many cases significantly reduces the number of samples required for an accurate interpolant through focussing on regions of rapid variation. Furthermore, the multi-fidelity modelling strategy using truncated sinuous antennas may also be applied to other log-periodic antenna structures — especially structures where the self-complementary constraint is relaxed to allow for uni-directional radiation patterns.

6 | ACKNOWLEDGEMENT

The authors acknowledge the financial support of the National Research Foundation (NRF) of South Africa, as well as that of the EUROSA project (https://www.uantwerpen.be/en/projects/eurosa/). Computations were performed using the University of Stellenbosch's HPC1 (Rhasatsha): http://www.sun.ac.za/hpc.

References

1. Welch J., Backer D., Blitz L., et al. The Allen Telescope Array: The First Widefield, Panchromatic, Snapshot Radio Camera for Radio Astronomy and SETI. *Proc. IEEE.* 2009;97(8):1438-1447.

2. Dewdney P. E., Hall P. J., Schilizzi R. T., Lazio T. J. L. W. The Square Kilometre Array. *Proc. IEEE.* 2009;97(8):1482 - 1496.

3. Yang J., Pantaleev M., Billade B., et al. A Compact Dual-Polarized 4-Port Eleven Feed With High Sensitivity for Reflectors Over $0.35 - 1.05$ GHz. *IEEE Trans. Antennas Propag.* 2015;63(12):5955-5960.

4. Gawande R., Bradley R. Towards an Ultra Wideband Low Noise Active Sinuous Feed for Next Generation Radio Telescopes. *IEEE Trans. Antennas Propag.* 2011;59(6):1945-1953.

5. DuHammel R. H., Isbell D. E. Broadband Logarithmically Periodic Antenna Structures. *1957 IRE National Convention Record.* 1957;1:119-128.

6. De Villiers D. I. L. Initial Study of a Pyramidal Sinuous Antenna as a Feed for the SKA Reflector System in Band-1. In: Antennas and Propagation Soc. Int. Symp.; July, 2017; San Diego, CA, USA:555 - 556.

7. Lehmensiek R., Theron I. P., Villiers D. I. L. Deriving an Optimum Mapping Function for the SKA Shaped Offset Gregorian Reflectors. *IEEE Trans. Antennas Propag.* 2015;63(11):4658-4666.

8. Cuyt A., Louw R., Segers C., De Villiers D. I. L. Towards blended rational interpolation of multi-fidelity antenna data. In: Proc. Int. Conf. Electromagn. Adv. Appl. (ICEAA); September, 2017; Verona, Italy.

9. Otoshi Tom Y. *Noise Temperature Theory and Applications for Deep Space Communications Antenna Systems.* Artech House; 2008.

10. Kildal P.-S. *Foundations of Antennas: A Unified Approach.* Studentlitteratur AB; 2000.

11. Rao Sudhakar, Shafai Lotfollah, Sharma Satish Kumar, eds. *Handbook of Reflector Antennas and Feed Systems: Theory and design of reflectors.* Boston, MA, USA: Artech house; 2013.

12. De Villiers D. I. L., Lehmensiek R. Rapid Calculation of Antenna Noise Temperature in Offset Gregorian Reflector Systems. *IEEE Trans. Antennas Propag.* 2015;63(4):1564-1571.

13. De Villiers D. I. L. Fast Parametric Modeling of Radio Astronomy Reflector Antenna Noise Temperature. *IEEE Trans. Antennas Propag.* 2016;64(6):2522-2526.

14. Miller E. K. Model-based parameter estimation in electromagnetics: Part I. Background and theoretical development. *IEEE Antennas Propag. Mag.* 1998;40(1):42-52.

15. Steenkamp N., Villiers D. I. L., Mutonkole N. Wideband Pyramidal Sinuous Antenna for Reflector Antenna Applications. In: European Conf. Antennas and Propagat.; April, 2017; Paris, France:2291 - 2295.

16. Altair Development S.A. (Pty) Ltd, Stellenbosch, South Africa. FEKO, Suite 14.0.

17. Berrut J.-P. Rational functions for guaranteed and experimentally well-conditioned global interpolation. *Comput. Math. Appl.* 1988;15:1-16.

18. Cuyt Annie. Approximation Theory. In: Higham N., ed. *Princeton Companion to Applied Mathematics*, Princeton University Press 2015 (pp. 248–262).

19. Nguyen Hoa Thang, Cuyt Annie, Salazar Celis Oliver. Comonotone and coconvex rational interpolation and approximation. *Numerical Algorithms.* 2011;58(1):1–21.

20. Deschrijver Dirk, Dhaene Tom, Celis Oliver Salazar, Cuyt Annie. Rational Modeling Algorithm for Passive Microwave Structures and Systems:37–43. Berlin, Heidelberg: Springer Berlin Heidelberg 2012.

21. Lorentz G.G. *Bernstein polynomials.* Chelsea Publishing Co., New York; second ed.1986.

22. Couckuyt I., Dhaene T., Demeester P. *ooDACE, a* MATLAB *Kriging toolbox: Getting started.* : Gent University, Gent, Belgium; 2013.

23. Li X. R., Zhao Z. Evaluation of estimation algorithms part I: Incomprehensive measures of performance. *IEEE Trans. Aerosp. Electron. Syst.* 2006;42(4):1340-1358.